A better understanding of the molecular basis of cancer would help develop targeted therapeutic agents against druggable genetic aberrations identified in cancer genomes.[7,8] Tyrosine kinase inhibitors (TKIs) that target anaplastic lymphoma kinase (ALK) are particularly effective in the treatment of a distinct subset of lung adenocarcinoma carrying *ALK* fusions.[9] *FIG-ROS1*, the first identified targetable fusion kinase in CC, has so far been reported in two patients.[10] Very recently, a novel kinase fusion, *FGFR2-BICC1*, was detected in two CC cases.[11] Thus, only a few cases harboring targetable fusion kinase genes have been reported, and the clinical characteristics of fusion-positive CC cases have not yet been described.

In the present study, we identified fibroblast growth factor receptor 2 (*FGFR2*) rearrangements including a novel *FGFR2-AHCYL1* fusion using whole transcriptome high-throughput sequencing of tumor specimens, and determined the prevalence of *FGFR2* rearrangements in CC. Our data indicate that *FGFR2*-fusions arise exclusively in ICC. *In vitro* studies suggest that *FGFR2* fusion kinase is a promising candidate for targeted therapy in CC.

Materials and Methods

Clinical Samples. Clinical specimens of cholangiocarcinoma, gastric cancer, hepatocellular carcinoma, and colorectal cancer were provided by the National Cancer Center Biobank, Japan. Total RNA was extracted from grossly dissected, snap-frozen tissue using RNAspin (GE Healthcare, Little Chalfont, UK) according to the manufacturer's instructions, and RNA quality was examined using a Bioanalyzer 2100 (Agilent Technologies, Santa Clara, CA). The study protocol was approved by the Ethics Committee of the National Cancer Center, Tokyo, Japan.

Analysis of Whole Transcriptome Sequence Data. Complementary DNA (cDNA) libraries composed of 150-200 bp inserts were prepared from 2 μg of total RNA using the TruSeq RNA Sample Preparation Kit (Illumina, San Diego, CA). The libraries were subjected to paired-end sequencing of 50-100 bp fragments on the HiSeq2000 instrument (Illumina) according to the manufacturer's instructions. Paired-end reads were mapped to known RNA sequences in the RefSeq, Ensembl, and LincRNA databases using the Bowtie program (v. 0.12.5) as basically described previously.[12] The detailed algorithm for fusion transcript detection is described in the Supporting Methods.

RT-PCR and Quantitative Real-Time PCR. Total RNA was reverse-transcribed to cDNA using SuperScript III (Life Technologies, Carlsbad, CA). The cDNA was subjected to PCR amplification using Ex-Taq (Takara Bio, Tokyo, Japan) with the following primers: FR2AHC-CF (GGACTCGCCAGAGATATCAACAATATAGAC) and FR2AHC-CR (GGACTG TGAGATCGAGCGAGAC) for *FGFR2-AHCYL1* fusion, FR2BIC-CF2 (GTGTTAATGTGGGAGATCT TCACTTTAGG) and FR2BIC-CR2 (CATCCATCTT CAGTGTGACTCGATTG) for *FGFR2-BICC1* fusion, FIG-e2CF1 (ACTGGTCAAAGTGCTGACTCTGGT) and ROS-e36CR2 (CAGCAAGAGACGCAGAGT-CAGTTT) for *FIG-ROS1* fusion, ACTB-S (CAAGA-GATGGCCACGGCTGCT) and ACTB-A (TCCTTC TGCATCCTGTCGGCA) for *β-actin*. The PCR products were directly sequenced by Sanger sequencing using the BigDye terminator kit (Life Technologies). The expression of the *FGFR2* transcript was assayed by quantitative real-time PCR (qPCR) using the LC480 thermal cycler (Roche, Penzberg, Germany). *FGFR2* expression was normalized to β-actin expression. Primers used for qPCR are as follows: FGFR2 (Fwd-GGACCCAAAATGGGAGTTTC, Rev-ACCACTTG CCCAAAGCAA), β-actin (Fwd-CCAACCGCGAGA AGATGA, Rev-CCAGAGGCGTACAGGGATAG).

Fluorescent* In Situ *Hybridization. To identify *FGFR2* rearrangements, break-apart fluorescent *in situ* hybridization (FISH) was performed on formalin-fixed, paraffin-embedded tumors using BAC clones corresponding to the 5′ (RP11-78A18) and 3′ (RP11-7P17) sequences flanking the *FGFR2* gene and labeled by nick translation in green and red, respectively.

Immunohistochemistry. Four-micrometer-thick sections from formalin-fixed paraffin-embedded block were used for immunohistochemistry. Epitope retrieval was performed with trypsin (T7168, Sigma, St. Louis,

Address reprint requests to: Tatsuhiro Shibata, M.D., Ph.D., Division of Cancer Genomics, National Cancer Center Research Institute, 5-1-1, Tsukiji, Chuo-ku, Tokyo, 104-0045, Japan. E-mail: tashibat@ncc.go.jp; fax: +81-3-3248-2463.

View this article online at wileyonlinelibrary.com.
DOI 10.1002/hep.26890
Potential conflict of interest: Dr. Okusaka is on the speakers' bureau for and received grants from Novartis and Pfizer.
Additional Supporting Information may be found in the online version of this article.

MO) for 20 minutes at pH 7.7. The slides were then washed with phosphate-buffered saline (PBS) and incubated overnight with FGFR2 antibody at 4°C (1:500, ab10648, Abcam, Cambridge, UK). Immunoreactions were detected using the EnVision-FLEX system (DAKO, Glostrup, Denmark).

cDNA Cloning and Generation of Kinase-Deficient Mutants. The full-length *FGFR2-AHCYL1* and *FGFR2-BICC1* cDNAs were isolated from the corresponding tumor specimens by RT-PCR using PrimeSTAR GXL polymerase (Takara Bio) and primers FGFR2-H5F1 (ATGGTCAGCTGGGGTCGTTTCA TCTGCCTGGTCG), AHCYL-H6R1 (GTATCTGTA ATAATTAGGTTTGAATGGCCC), and BICC1-H6R1 (CCAGCGGCCACTGACACTAGCAATGTCTGA). *EZR-ROS1* cDNA was reported previously.[13] Each cDNA was subcloned into a pMXs vector (Cell Biolabs, San Diego, CA) to generate recombinant retrovirus expressing the fusion protein with a FLAG epitope tag. The kinase activity-deficient mutants were constructed by replacing tyrosine with phenylalanine at codons 568 and 569 in the *FGFR2-AHCYL1* and *FGFR2-BICC1* genes using a PrimeSTAR site-directed mutagenesis kit (Takara Bio).

Transforming Activity of FGFR2 Fusions. Mouse NIH3T3 fibroblast cells were infected with EZR-ROS1, FGFR2-AHCYL1, FGFR2-AHCYL1-KD, FGFR2-BICC1, or FGFR2-BICC1-KD-expressing retroviruses. Quantification of anchorage-independent growth was performed on day 12 in soft agar with the CytoSelect-96 kit (Cell Biolabs) in the presence or absence of FGFR inhibitors BGJ398 (#S2183, Selleck, Houston, TX) and PD173074 (#S1264, Selleck). The compound solution was added to the top layer of soft agar every 3 days.

Subcutaneous Transplantation in Immune-Compromised Mice. A total of 1×10^6 transduced NIH3T3 cells were injected subcutaneously into nude mice (BALB/c-nu/nu, CLEA Japan, Tokyo, Japan). Tumor formation was measured after 18 days. All animal procedures were performed with the approval of the Animal Ethics Committee of the National Cancer Center, Tokyo, Japan.

Immunoblot Analysis. To analyze signaling, retrovirally transduced NIH3T3 cells were serum-starved for 2 hours, after which vehicle (DMSO), BGJ398, or PD173074 was added for a further 2 hours. The culture medium was then changed to standard medium containing 10% fetal bovine serum (FBS) for 10 minutes. Whole cell lysates were subjected to sodium dodecyl sulfate-polyacrylamide gel electrophoresis (SDS-PAGE) followed by transfer to a PVDF membrane. Western blot detection was performed with the WesternBreeze Chemiluminescent Immunodetection kit (Life Technologies) using primary antibodies against FLAG tag (#1E6, Wako Chemicals, Tokyo, Japan), phospho-FGFR1-4 (Tyr653, 654) (#AF3285, R&D Systems, Minneapolis, MN), STAT3 (#610189, BD, Becton Drive, NJ), phospho-STAT3 (Tyr705) (#9138, Cell Signaling Technology, Danvers, MA), p44/42 MAPK (#4695, Cell Signaling Technology), and phospho-p44/42 MAPK (Thr202/Tyr204) (#9106, Cell Signaling Technology), AKT1 (#2967, Cell Signaling Technology), and phospho-AKT (Ser473) (#4051, Cell Signaling Technology).

Statistical Analysis. All data analyses were performed using JMP v. 8.02 (SAS Institute, Cary, NC). Fisher's exact test was used for categorical data, and the Student *t*-test was used for continuous data. Overall survival, measured from the date of surgery, was determined using the Kaplan-Meier method, and survival difference was compared using the log-rank test. Two-sided significance level was set at $P < 0.05$.

Results

Identification of a Novel FGFR2 Fusion Gene. Whole transcriptome high-throughput sequencing of tumor specimens is one of the most effective methods for the identification of fusion oncogenes. Eight primary cholangiocarcinomas without *KRAS/BRAF* mutations or *FIG-ROS1* fusion (Supporting Table 1) were analyzed to identify novel molecular alterations by massively parallel paired-end transcriptome sequencing. Aberrant paired reads that mapped to different transcription units were identified, and 17 potential fusion transcripts were predicted by our algorithm[12] (Supporting Table 2). Sequence reads spanning the junctions of eight fusion candidate transcripts indicated in-frame gene fusion (Fig. 1A-C; Supporting Table 3) and were verified by direct sequencing of RT-PCR products spanning the breakpoints. Among these, fusion transcripts of the receptor kinase gene were detected as *FGFR2-AHCYL1*, *FGFR2-BICC1*, *AHCYL1-FGFR2*, and *BICC1-FGFR2*. However, two transcripts of *AHCYL1-FGFR2* and *BICC1-FGFR2* did not encode a functional protein of relevance to cancer, and conversely *FGFR2-AHCYL1* and *FGFR2-BICC1* were predicted to form chimeric proteins carrying the kinase domain of FGFR2 (Fig. 1D). Transcriptome sequencing showed a specific increase in the expression of the fused 3′ portion of *AHCYL1* and *BICC1* (Supporting Fig. 1A,B). Therefore, the formation of *FGFR2-AHCYL1* or *FGFR2-BICC1* might play important roles in cancer transformation.

From the tumor specimens, CC64 and CC73, we obtained cDNAs corresponding to *FGFR2-AHCYL1*

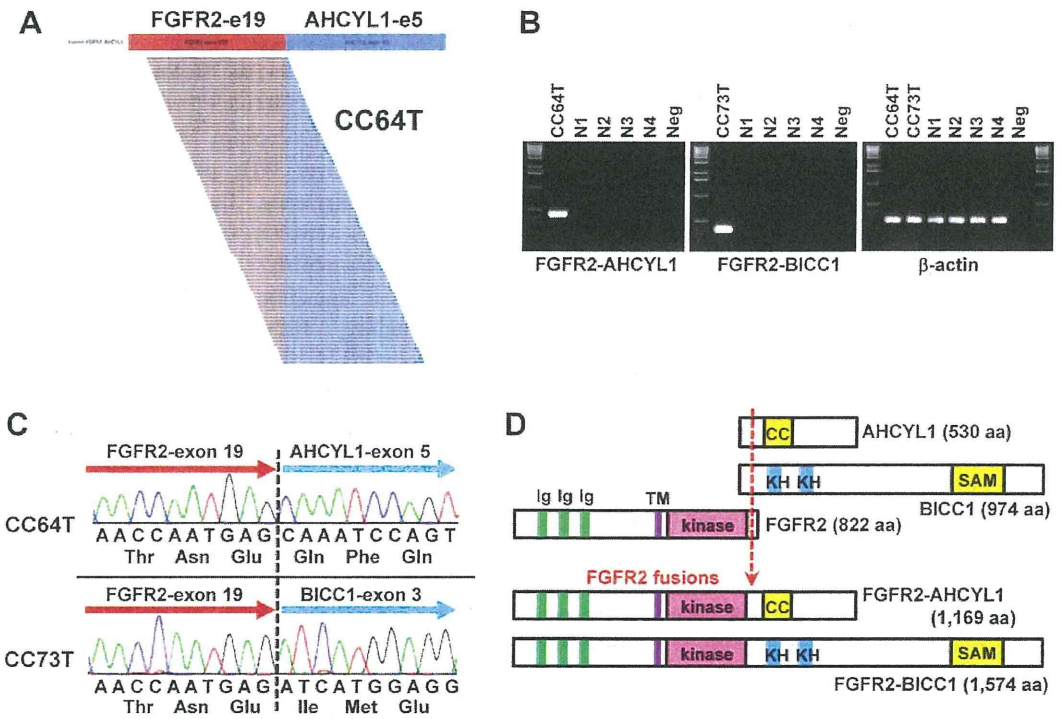

Fig. 1. *FGFR2* fusion genes in cholangiocarcinoma. (A) Junction reads representing *FGFR2-AHCYL1* fusion transcripts in CC64T samples. (B) Confirmation of tumor specific fusion transcripts by RT-PCR. Fusion transcripts were detected only in tumor tissues (CC64T and CC73T), but not in normal liver tissues (N1-N4). Neg: no template. β-Actin expression was used as a control. (C) Sanger sequencing of the RT-PCR product validated in-frame fusion transcripts. (D) Schematic representation of FGFR2-AHCYL1 and FGFR2-BICC1 fusion proteins. Ig: immunoglobulin-like domain, TM: transmembrane domain, kinase: protein tyrosine kinase domain, CC: coiled-coil domain, KH: K homology RNA binding domain, SAM: sterile alpha motif. The dotted vertical line indicates break points.

and *FGFR2-BICC1* encoding 1,169 and 1,574 amino acids, respectively. The chimeric genes consisted of the in-frame fusion of the *FGFR2* amino terminus (exons 1-19) and the *AHCYL1* carboxyl terminus (exons 5-21) or the *BICC1* carboxyl terminus (exons 3-21) (Fig. 1C,D; GenBank/DDBJ accession numbers AB821309 and AB821310). *FGFR2-AHCYL1* is a novel *FGFR2* fusion. *AHCYL1* encodes an S-adenosyl-L-homocysteine hydrolase and inositol 1,4,5-trisphosphate binding protein, and contains a coiled-coil motif in the central domain.[14] *BICC1* encodes an RNA binding protein with a sterile alpha motif (SAM) protein-interaction and dimerization module at the carboxyl terminus.[15] The FGFR2-AHCYL1 and FGFR2-BICC1 fusion proteins are likely to form homodimers through the coiled-coil motif of AHCYL1 and the SAM motif[16] of BICC1, respectively. *FGFR2*, *AHCYL1*, and *BICC1* mapped to chromosome 10q26.1, 1p13.2, and 10q21.1, respectively (Fig. 2A). *FGFR2* and *BICC1* are located on the long arm of chromosome 10 in opposite directions, suggesting that the *FGFR2-BICC1* fusion is generated by intrachromosomal inversion (Supporting Fig. 1B). Gross rearrangement of the *FGFR2* gene locus was verified by FISH with break-apart probes, which showed a split in the signals of the probes flanking the *FGFR2* breakpoint in CC64 and CC73 tumors (Fig. 2B).

Prevalence of FGFR2 Fusions. RT-PCR and Sanger sequencing analysis of 102 cholangiocarcinoma specimens (66 ICCs and 36 ECCs) from Japanese individuals, including eight who had been subjected to whole transcriptome sequencing, identified seven *FGFR2-AHCYL1*-positive and two *FGFR2-BICC1*-positive cases (Table 1; Supporting Table 4). The nine *FGFR2*-fusion-positive cases were ICC type tumors (9/66, 13.6%). *KRAS* mutations were detected in 19 cases (19/102, 17.8%) and *BRAF* mutations in one (1/102, 1%); these mutations were mutually exclusive with the *FGFR2* fusions (Fig. 3A; Supporting Table 4). Although two cases of *FIG-ROS1* fusion (2/23, 8.7%) have been reported by other researchers in cholangiocarcinoma,[10] we did not detect such fusion in this cohort. No significant differences in age, gender, tumor differentiation, clinical stage, and prognosis were detected between fusion-positive and -negative cases. (Table 2, Fig. 3B). Overall survival of ICC cases

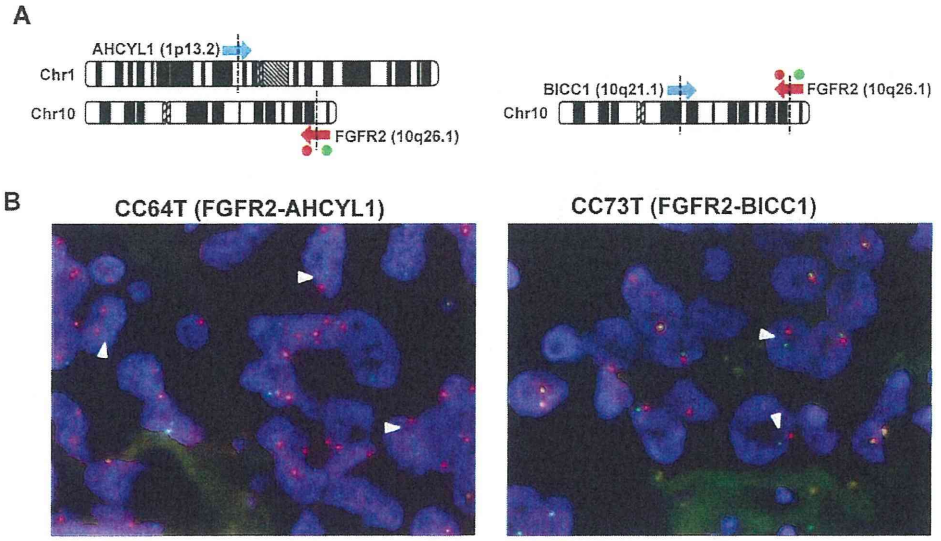

Fig. 2. Detection of *FGFR2* rearrangements. (A) Schematic representation of *FGFR2* gene rearrangements: *FGFR2-AHCYL1* (left) and *FGFR2-BICC1* (right). Arrows indicate the position and direction of the fused genes. Green and red spots indicate the genomic location of 5′ and 3′ FISH probes for the *FGFR2* gene. (B) Representative FISH pattern of *FGFR2* probes in *FGFR2-AHCYL1* and *FGFR2-BICC1*-positive cases. Arrows indicate a split of 5′ green and 3′ red signals.

also showed no great distinction between the two groups. However, fusion positive cases had a propensity for hepatitis virus infection (Table 2). Expression of *FGFR2* mRNA was significantly higher in fusion-positive cases than in fusion-negative ones (Supporting Fig. 2). Especially, *KRAS/BRAF* mutant cases showed reduced *FGFR2* expression. This might afford collateral evidence of mutually exclusive relationships between *FGFR2* fusion and *KRAS/BRAF* mutation. Immunohistological analysis revealed prominent FGFR2 protein expression at both cytoplasm and plasma membrane in fusion-positive cases (Supporting Fig. 3). We further screened 212 gastric cancers, 149 colorectal cancers, and 96 hepatocellular carcinomas by RT-PCR for the presence of these FGFR2 fusion transcripts. The *FGFR2-BICC1* fusion gene was detected in one colorectal cancer (0.7%) and one hepatocellular carcinoma (1.0%). These fusion-positive non-ICC cases were also hepatitis virus-positive (Table 1).

***FGFR2 Fusions Transform NIH3T3 Cells Both* In Vitro *and* In Vivo.** To assess the oncogenic activity of the FGFR2 fusion proteins, stable NIH3T3 clones expressing the retrovirally transfected wild-type fusion proteins or their kinase activity-deficient mutants (KD mutant) were established. As shown in Fig. 4A, wild-type FGFR2-AHCYL1 or FGFR2-BICC1-expressing cells showed anchorage-independent colony formation in soft agar, which was severely suppressed in KD mutant expressing cells. Subcutaneous transplantation of these clones into immunodeficient mice resulted in the formation of tumors from FGFR2-AHCYL1 and FGFR2-BICC1 expressing clones, whereas those expressing KD mutants did not form tumors (Fig. 4B).

To investigate the mechanisms by which the FGFR2 fusion drives oncogenesis, downstream FGFR signaling was analyzed *in vitro* (Fig. 5A; Supporting Fig. 4). The wild-type fusion expressing cells showed constitutive tyrosine phosphorylation in the activation loop of the FGFR kinase domain. FGFR2 signaling activates multiple downstream pathways, including RAS/MAPK and PI3K/AKT.[17] Immunoblot analysis revealed that activation of MAPK, but not AKT or STAT3, was induced in clones expressing FGFR2-AHCYL1 and FGFR2-BHCC1. These results indicate that FGFR2 fusion proteins activate

Table 1. Clinical Features of FGFR2 Fusion Positive Cases

FGFR2 fusion	Gender	Age	Virus status	Pathlogy	Differentiation
FGFR2-AHCYL	F	72	HCV	ICC	mod
FGFR2-AHCYL	F	59		ICC	well
FGFR2-AHCYL	M	62	HCV	ICC	mod
FGFR2-AHCYL	M	73		ICC	well
FGFR2-AHCYL	F	52		ICC	mod
FGFR2-AHCYL	M	59		ICC	well
FGFR2-AHCYL	F	49		ICC	mod
FGFR2-BICC1	M	65	HBV	ICC	mod
FGFR2-BICC1	F	68		ICC	well
FGFR2-BICC1	F	66	HCV	CRC	mod
FGFR2-BICC1	F	46	HBV	HCC	por

ICC: Intrahepatic cholangiocarcinoma
CRC: colorectal cancer
HCC: hepatocellular carcinoma

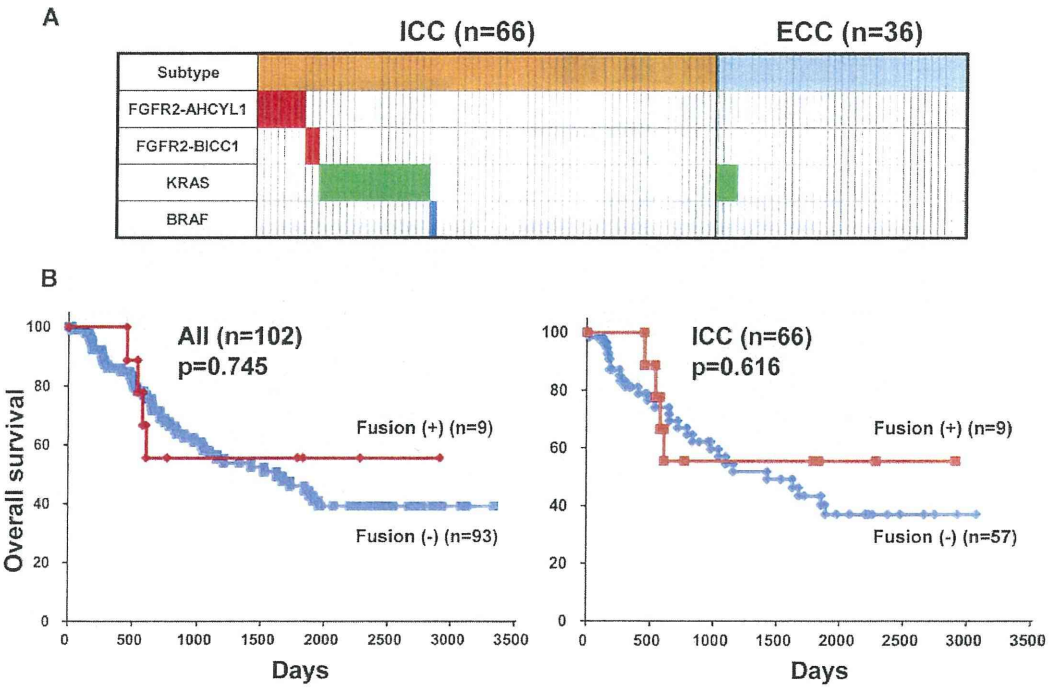

Fig. 3. Clinical subtypes in cholangiocarcinoma. (A) Distribution of genomic alterations. *FGFR2* fusion, *KRAS* mutation, and *BRAF* mutation among ICC and ECC cases are indicated by red, green, and blue, respectively. (B) Overall survival curve stratified by *FGFR2* fusions in all cholangiocarcinoma cases and ICC cases (Kaplan-Meier method). The outcome was not significantly different between *FGFR2* fusion-positive and -negative cases (log-rank test).

canonical FGFR signaling and confer anchorage-independent growth and *in vivo* tumorigenesis, both of which are hallmarks of cellular transformation.

FGFR2 Fusions Are Potential Therapeutic Targets in Cholangiocarcinoma. Next, we examined the sensitivity of *FGFR2* fusion-driven tumor cells to two specific FGFR inhibitors, BGJ398 and PD173074, which selectively inhibit FGFR tyrosine kinase activity.[18,19] These compounds significantly inhibited the phosphorylation of MAPK and reduced *in vitro* anchorage-independent colony formation to the level observed in KD mutant expressing cells (Fig. 5B).

Discussion

FGFR genes are involved in multiple biological processes, ranging from cell transformation, angiogenesis, and tissue repair, to embryonic development. Activating point mutations and amplification of *FGFR* gene members have been explored as therapeutic targets in a wide range of tumors, including bladder, gastric, and lung cancers[20,21]; however, amplification of *FGFR* genes is uncommon in ICC.[22] Diverse fusions involving the *FGFR* gene family have also been reported in hematological and solid cancers[10,11,23,24] and some have shown sensitivity to FGFR inhibition.

The identification of two recurrent *FGFR2* fusions (*FGFR2-AHCYL1* and *FGFR2-BICC1*) that are mutually exclusive with *KRAS/BRAF* mutations warrants a new molecular classification of cholangiocarcinoma and suggests a novel therapeutic approach in cholangiocarcinomas driven by these fusions. Wu et al.[11] recently detected the *FGFR2-BICC1* fusion gene in two cholangiocarcinoma cases, although its prevalence

Table 2. Association Between Clinical Features and FGFR2 Fusion

Clinical factors		Number of fusion positive case	Number of fusion negative case	*P* Value
Gender	Male	4	61	0.207
	Female	5	32	
Age (average)		62.1	66.1	0.104
Virus status	Hepatitis virus positive	3	9	0.035
	Hepatitis virus negative	6	84	
Differentiation	Well	4	21	0.367
	Mod	5	60	
	Poor	0	5	
Stage	I	1	2	0.463
	II	2	14	
	III	2	30	
	IV	4	23	

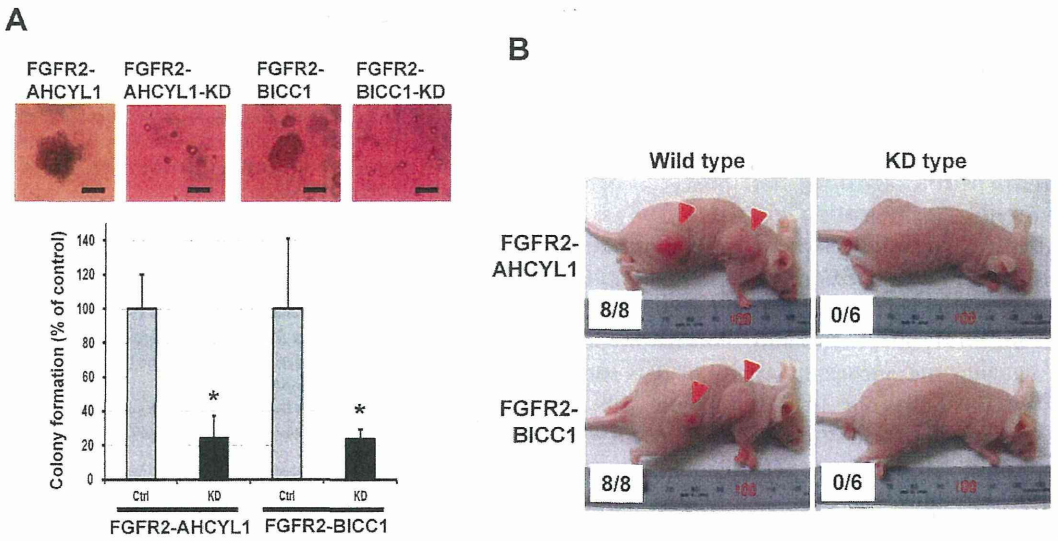

Fig. 4. Oncogenic activity of FGFR2 fusion proteins. (A) Soft agar colony formation in kinase activity-deficient (KD) mutants. The percentage (±SD) of colonies with FGFR2 fusions and their KD mutant transfectants are plotted. $*P < 0.05$. A representative image of colonies expressing wild-type and KD FGFR2 fusions is shown (scale bar = 100 μm). (B) Representative images of mice subcutaneously transplanted with NIH3T3 cells expressing wild-type and KD FGFR2 fusions. The number of tumors per injection in each transfectant is shown.

in cholangiocarcinoma has been lacking. The present study showed a high prevalence of *FGFR2* fusion genes in the intrahepatic subtype of cholangiocarcinoma. Although two cases of another kinase fusion, *FIG-ROS1* (2/23, 8.7%), have been reported by other researchers in CC,[10] we did not detect such fusion in this study. As cholangiocarcinoma is a heterogeneous disease, some epidemiological or clinical specificity may be ascribable to the *FIG-ROS1* fusion. However, no detailed pathological information of the patients was stated in that study. Further investigation is needed to clarify the whole picture of driver fusion genes in CC. Association between *FGFR2* fusion positivity and hepatitis virus infection may suggest an involvement of the virus in the chromosomal rearrangements in CC. However, rare observation of *FGFR2* fusion in hepatocellular carcinoma argues for further analysis of genetic rearrangements.

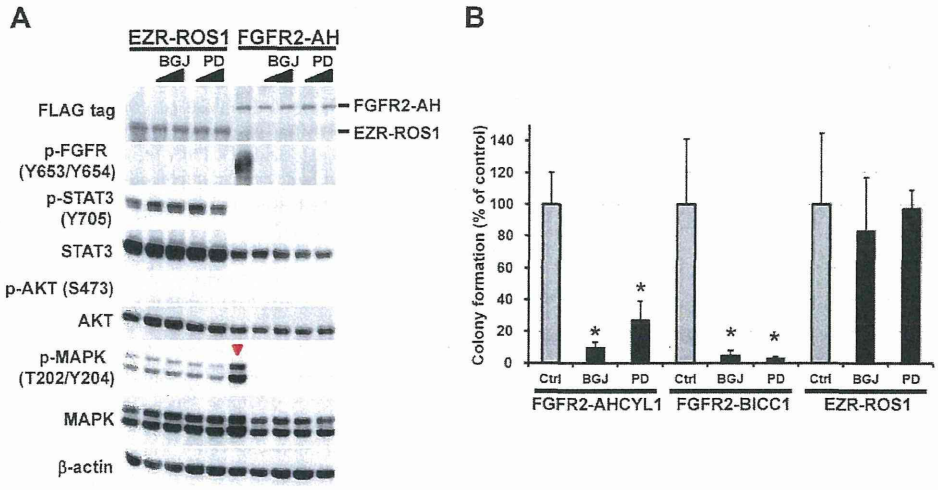

Fig. 5. FGFR inhibitors block signaling in FGFR2-fusion-expressing cells. (A) Activation of FGFR2 and MAPK by FGFR2-AHCYL1 and its suppression by FGFR inhibitors. Lysates from NIH3T3 cells expressing FGFR2-AHCYL1 or EZR-ROS1 (control) treated with vehicle (DMSO), 0.2 and 1 μM BGJ398, and 0.2 and 1 μM PD173074 were immunoblotted with the relevant antibodies. β-Actin was used as a loading control. (B) Anchorage-independent growth of NIH3T3 cells expressing FGFR2 fusions and its suppression by FGFR inhibitors (BGJ: BGJ398 and PD: PD173074). The percentage (±SD) of colonies formed in the presence of FGFR2 inhibitors (0.2 μM) with respect to those formed by DMSO-treated cells are plotted. The NIH3T3 clone expressing EZR-ROS1 was used as a negative control for FGFR inhibitors. $*P < 0.05$.

Overexpression of the FGFR2 fusion protein hyperactivate one of the canonical signaling events downstream of FGFR. This contrast with other FGFR fusion proteins, FGFR1-TACC1 and FGFR3-TACC3 in glioblastoma,[24] which fail to activate canonical downstream MAPK signaling, but induce aneuploidy and oncogenic transformation.[9]

Based on the specific relevant genomic alterations, TKIs have been developed into effective therapies.[7,8] We showed that small molecule FGFR inhibitors, BGJ398 and PD173074, efficiently blocked the downstream signaling and oncogenic activity of ICC-specific *FGFR2* fusions. By the high-throughput cell line profiling assay, amplifications or mutations of *FGFR* genes in cancer cell lines have been reported to predict sensitivity to the selective pan-FGFR inhibitor BGJ398.[25] This drug is currently in a phase I study in patients of advanced solid tumors with FGFR1/2 amplification or FGFR3 mutation (Novartis, Basel, Switzerland; ClinicalTrials.gov identifier: NCT01004224). Clinical investigations, akin to those conducted in other solid tumors with oncogenic fusion kinases, such as *EML4-ALK*,[26] are warranted to examine the efficacy of FGFR inhibitors for the treatment of defined subset of cholangiocarcinoma harboring *FGFR2* fusions.

Acknowledgment: We thank S. Wakai, H. Shimizu, S. Ohashi, W. Mukai, T. Urushidate, and N. Okada of the National Cancer Center for excellent technical assistance.

Author Contributions: Sequencing and data analysis: Y.T., N.H., H.N., F.H.; Molecular biological analysis: Y.A., F.H.; Clinical and pathological analysis: T.Shirota., H.O., K.F., K.S., T.O., T.K.; Article writing: Y.A., Y.T., F.H., T.S.; Study design: Y.A., Y.T., T. Shibata.

References

1. Razumilava N, Gores GJ. Classification, diagnosis, and management of cholangiocarcinoma. Clin Gastroenterol Hepatol 2013;11:13-21.
2. Khan SA, Thomas HC, Davidson BR, Taylor-Robinson SD. Cholangiocarcinoma. Lancet 2005;366:1303-1314.
3. Ong, CK, Subimerb C, Pairojkul C, Wongkham S, Cutcutache I, et al. Exome sequencing of liver fluke-associated cholangiocarcinoma. Nat Genet 2012;44:690-693.
4. Voss JS, Holtegaard LM, Kerr SE, Barr Fritcher EG, Roberts LR, Gores GJ, et al. Molecular profiling of cholangiocarcinoma shows potential for targeted therapy treatment decisions. Hum Pathol 2013; 44:1216-1222.
5. Hezel AF, Zhu AX. Systemic therapy for biliary tract cancers. Oncologist 2008;13:415-423.
6. Aljiffry M, Abdulelah A, Walsh M, Peltekian K, Alwayn I, Molinari M. Evidence-based approach to cholangiocarcinoma: a systematic review of the current literature. J Am Coll Surg 2009;208:134-147.
7. Mitelman F, Johansson B, Mertens F. The impact of translocations and gene fusions on cancer causation. Nat Rev Cancer 2007;7:233-245.
8. Ablain J, Nasr R, Bazarbachi A, de The H. The drug-induced degradation of oncoproteins: An unexpected Achilles' heel of cancer cells? Cancer Discov 2011;1:117-127.
9. Gerber DE, Minna JD. ALK inhibition for non-small cell lung cancer: from discovery to therapy in record time. Cancer Cell 2010;18:548-551.
10. Gu TL, Deng X, Huang F, Tucker M, Crosby K, Rimkunas V, et al. Survey of tyrosine kinase signaling reveals ROS kinase fusions in human cholangiocarcinoma. PLoS One 2011;6:e15640.
11. Wu YM, Su F, Kalyana-Sundaram S, Khazanov N, Ateeq B, Cao X, et al. Identification of targetable FGFR gene fusions in diverse cancers. Cancer Discov 2013; 3:636-647.
12. Kohno T, Ichikawa H, Totoki Y, Yasuda K, Hiramoto M, Nammo T, et al. KIF5B-RET fusions in lung adenocarcinoma. Nat Med 2012;18: 375-377.
13. Arai Y, Totoki Y, Takahashi H, Nakamura H, Hama N, Kohno T, et al. Mouse model for ROS1-rearranged lung cancer. PLoS One 2013; 8:e56010.
14. Ando H, Mizutani A, Matsu-ura T, Mikoshiba K. IRBIT, a novel inositol 1,4,5-trisphosphate (IP3) receptor-binding protein, is released from the IP3 receptor upon IP3 binding to the receptor. J Biol Chem 2003; 278:10602-10612.
15. Wessely O, Tran U, Zakin L, De Robertis EM. Identification and expression of the mammalian homologue of Bicaudal-C. Mech Dev 2001;101:267-270.
16. Kim CA, Bowie JU. SAM domains: uniform structure, diversity of function. Trends Biochem Sci 2003;28:625-628.
17. Brooks AN, Kilgour E, Smith PD. Molecular pathways: fibroblast growth factor signaling: a new therapeutic opportunity in cancer. Clin Cancer Res 2012;18:1855-1862.
18. Skaper SD, Kee WJ, Facci L, Macdonald G, Doherty P, Walsh FS. The FGFR1 inhibitor PD 173074 selectively and potently antagonizes FGF-2 neurotrophic and neurotropic effects. J Neurochem 2000;75:1520-1527.
19. Guagnano V, Furet P, Spanka C, Bordas V, Le Douget M, Stamm C, et al. Discovery of 3-(2,6-dichloro-3,5-dimethoxy-phenyl)−1-{6-[4-(4-ethyl-piperazin-1-yl)-phenylamino]-pyrimidin-4-yl}-1-methyl-urea (NVP-BGJ398), a potent and selective inhibitor of the fibroblast growth factor receptor family of receptor tyrosine kinase. J Med Chem 2011;54:7066-7083.
20. Turner N, Grose R. Fibroblast growth factor signaling: from development to cancer. Nat Rev Cancer 2010;10:116-129.
21. Weiss J, Sos ML, Seidel D, Peifer M, Zander T, Heuckmann JM, et al. Frequent and focal FGFR1 amplification associates with therapeutically tractable FGFR1 dependency in squamous cell lung cancer. Sci Transl Med 2010;2:62ra93.
22. Sia D, Hoshida Y, Villanueva A, Roayaie S, Ferrer J, Tabak B, et al. Integrative molecular analysis of intrahepatic cholangiocarcinoma reveals 2 classes that have different outcomes. Gastroenterology 2013; 144:829-840.
23. Chase A, Grand FH, Cross NC. Activity of TKI258 against primary cells and cell lines with FGFR1 fusion genes associated with the 8p11 myeloproliferative syndrome. Blood 2007;110:3729-3734.
24. Singh D, Chan JM, Zoppoli P, Niola F, Sullivan R, Castano A, et al. Transforming fusions of FGFR and TACC genes in human glioblastoma. Science 2012;337:1231-1235.
25. Guagnano V, Kauffmann A, Wöhrle S, Stamm C, Ito M, Barys L, et al. FGFR genetic alterations predict for sensitivity to NVP-BGJ398, a selective pan-FGFR inhibitor. Cancer Discov 2012;2:1118-1133.
26. Kwak EL, Bang YJ, Camidge DR, Shaw AT, Solomon B, Maki RG, et al. Anaplastic lymphoma kinase inhibition in non-small-cell lung cancer. N Engl J Med 2010;363:1693-1703.

OPEN ACCESS Freely available online

PLOS | ONE

Concurrent Activation of Acetylation and Tri-Methylation of H3K27 in a Subset of Hepatocellular Carcinoma with Aggressive Behavior

Akimasa Hayashi[1,2], Naoko Yamauchi[1], Junji Shibahara[1], Hiroshi Kimura[3], Teppei Morikawa[1], Shumpei Ishikawa[4], Genta Nagae[2], Akihiro Nishi[6], Yoshihiro Sakamoto[5], Norihiro Kokudo[5], Hiroyuki Aburatani[2], Masashi Fukayama[1]*

1 Department of Pathology, Graduate School of Medicine, The University of Tokyo, Tokyo, Japan, **2** Genome Science Division, Research Center for Advanced Science and Technology (RCAST), The University of Tokyo, Tokyo, Japan, **3** Biomolecular Networks Laboratories Group, Graduate School of Frontier Biosciences, Osaka University, Suita, Japan, **4** Department of Genomic Pathology, Medical Research Institute, Tokyo Medical and Dental University, Tokyo, Japan, **5** Hepato-Biliary-Pancreatic Surgery Division, Department of Surgery, Graduate School of Medicine, The University of Tokyo, Tokyo, Japan, **6** Yale Institute for Network Science, New Haven, Connecticut, United States of America

Abstract

Analysis of acetylation and tri-methylation of the same residue of histone molecules might identify a subset of hepatocellular carcinoma (HCC) with aggressive behavior. In the present study, we examined acetylation and tri-methylation of lysine 27 on histone H3 (H3K27ac and H3K27me3, respectively) because these two modifications are known to exhibit opposite effects (enhancing and silencing) on gene expression. Neoplastic and non-neoplastic tissues from 198 HCC cases were immunostained with specific monoclonal antibodies against H3K27ac and H3K27me3. The stained tissues were evaluated by an image analyzing program to generate histological scores (H-scores, range 0–300), which were determined by multiplying the percentage of positive-stained cells with the classified immunohistochemical marker intensity (0–3). HCC tissues showed significantly higher H3K27ac (156.7±86.8) and H3K27me3 H-scores (151.8±78.1) compared with the background liver (40.3±33.0 and 64.7±45.6, respectively) (both $P<0.001$). The cases with H-scores of high-H3K27ac/high-H3K27me3 (n = 54) showed significant correlation with poor differentiation of morphology ($P<0.01$) and p53-positive staining ($P<0.05$), and poor prognosis ($P<0.01$). Confocal microscopy revealed segregated intranuclear localization of both modifications in the individual cancer cells: H3K27ac localization in central euchromatin regions and H3K27me3 in peripheral heterochromatin regions. Concurrent acetylation and methylation at H3K27 occurs in HCC cells in association with p53 abnormalities. These findings demonstrate that image analyzer-assisted H-scores of H3K27ac and H3K27me3 identified an aggressive subgroup of HCC, and could serve as a prognostic marker for HCC.

Citation: Hayashi A, Yamauchi N, Shibahara J, Kimura H, Morikawa T, et al. (2014) Concurrent Activation of Acetylation and Tri-Methylation of H3K27 in a Subset of Hepatocellular Carcinoma with Aggressive Behavior. PLoS ONE 9(3): e91330. doi:10.1371/journal.pone.0091330

Editor: Taro Yamashita, Kanazawa University, Japan

Received November 1, 2013; **Accepted** February 9, 2014; **Published** March 10, 2014

Funding: This work was supported by the grant, Technology development for drug discovery platform based on the epigenetic mechanism (P10005) from New Energy and Industrial Technology Development Organization (NEDO), Japan (http://www.nedo.go.jp/english/index.html). The funders had no role in study design, data collection and analysis, decision to publish, or preparation of the manuscript.

Competing Interests: The authors have declared that no competing interests exist.

* E-mail: mfukayama-tky@umin.net

Introduction

Hepatocellular carcinoma (HCC) is one of the major cancers worldwide [1]. HCC is especially common in Asia-Pacific countries and is ranked the fourth highest cause of death among cancers in Japan [2]. Despite recent advances in resection and ablation techniques, the recurrence rate after initial treatment is high and prognosis is poorer than other carcinomas [2,3]. Improved risk stratification and accurate individualized prediction of postoperative recurrence and survival can help guide patient counseling, follow-up scheduling, administration of adjuvant therapies, and design of clinical trials [4].

Accumulating evidence has shown that not only genetic but also epigenetic changes play crucial roles in the genesis and prognosis of cancer [5,6]. Global levels of several histone modifications, as well as histone modification enzymes, have clinical significance in several cancers [7–9]. A recent review on histone modifications and cancer also referred its potential that serves as a biomarker [10]. Previous studies in HCC demonstrated the clinical significance of individual histone methylation levels. High levels of tri-methylation of lysine 4 on histone H3 (H3K4me3) and tri-methylation of lysine 27 on histone H3 (H3K27me3) correlated with aggressive features and poor prognosis [11,12]. However, little is known about global histone acetylation levels in HCC. One immunohistochemical study revealed that the levels of acetylation of lysine 9 on histone 3 (H3K9ac) and acetylation of lysine 8 on histone 4 (H4K8ac) were higher in HCC than in non-cancerous liver, but the clinical significance remains unknown [13].

In this study, we focused on acetylation of lysine 27 on histone H3 (H3K27ac) and its relation with H3K27me3. H3K27ac is an active enhancer marker and reflects global cell-type-specific gene expression in various cancer cell lines [14]. H3K27me3 is another

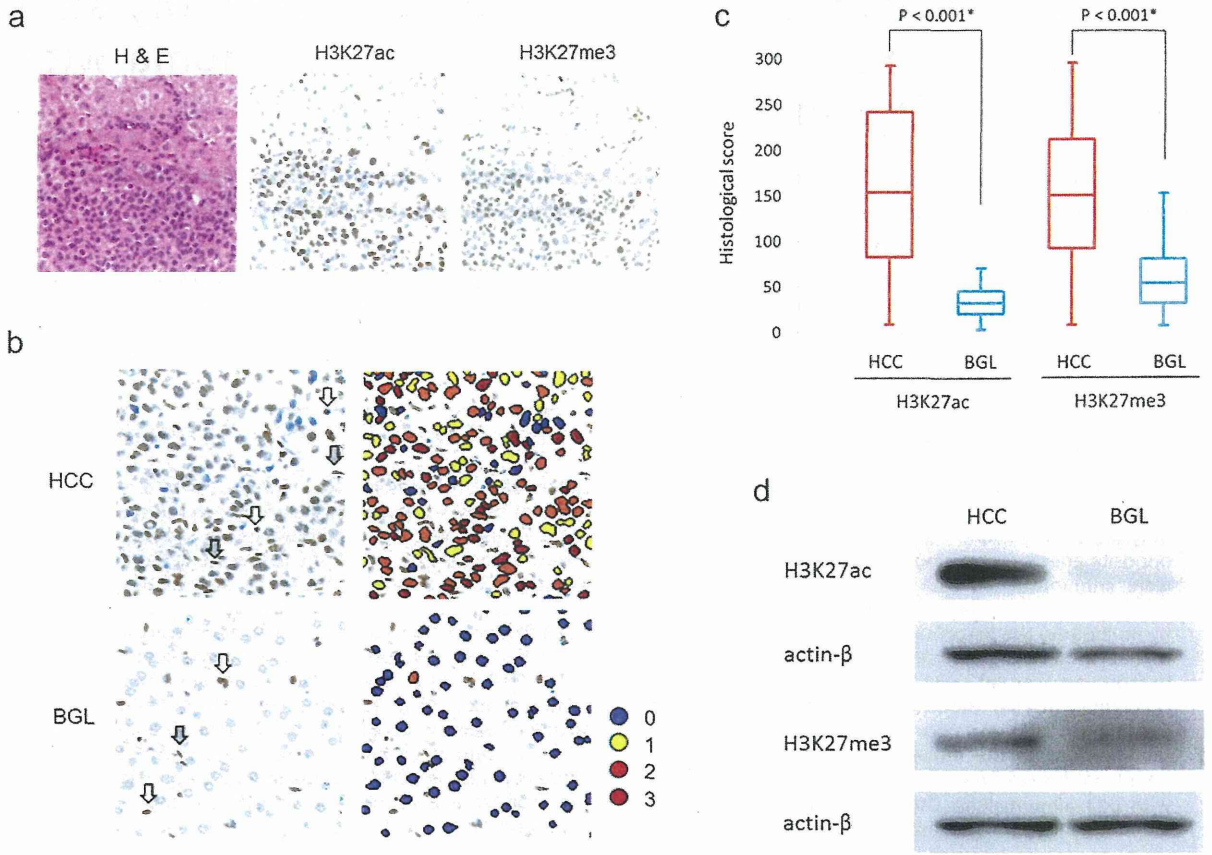

Figure 1. H3K27ac and H3K27me3 in HCC and background liver (BGL). (a) Images of hematoxylin and eosin (H&E), H3K27ac and H3K27me3 staining around the border between HCC and BGL. (b) Images of HCC and BGL samples by objective-quantitative analysis with Tissue Studio (Definiens AG, Munich, Germany). Each nucleus was assigned scores of 0 (negative), 1 (weakly positive), 2 (moderately positive) or 3 (strongly positive). Inflammatory cells (white arrows) and endothelial cells (gray arrows) were excluded in this analysis. (c) Distributions of histological scores (H-scores) for H3K27ac and H3K27me3 in HCCs and BGLs using box-plots. Statistical analyses were performed using the Mann-Whitney test. (d) Western blot showing increased levels of H3K27ac and H3K27me3 in HCCs compared with the matched non-cancerous liver. Actin-β was used as a loading control.
doi:10.1371/journal.pone.0091330.g001

histone modification of the same site, and acts instead as a silencer [15]. We evaluated both H3K27ac and H3K27me3 levels in HCC using specific monoclonal antibodies, and used digital slide scanner and image analyzing software to quantify the results as objectively as possible [16]. In addition, we examined nuclear localization of H3K27ac and H3K27me3 by double immunofluorescence in frozen sections. In evaluating the clinicopathological significance, we also assessed the status of p53 and β-catenin, two major HCC driver genes [17], because interplay between the cancer genome and epigenome is important, especially in HCC [6].

Materials and Methods

Ethics Statement

This study was approved by the University of Tokyo Institutional Ethical Committee. Clinical samples with written informed consent were collected under the University of Tokyo Institutional guidelines for the study of human tissues.

Tissue microarrays

A total of 198 primary HCC cases were retrieved from the archives of the Department of Pathology of The University of Tokyo Hospital to generate tissue microarrays (TMAs). Surgical resections were performed between 1995 and 2006 based on Makuuchi criterion for resection of HCC [18]. Resection samples were fixed with formalin and embedded in paraffin. Hematoxylin and eosin (H&E)-stained slides of all the cases were reviewed. Histological diagnosis was based on the most recent criteria proposed by the Liver Cancer Study Group of Japan [19]. TMAs were generated according to well-established procedures [20]. In brief, two tissue cores (2 mm diameter each) were punched out of each donor paraffin block and transferred to each of the recipient TMA blocks. TMAs for the paired background livers were also produced.

Frozen samples

Frozen samples were used for western blotting and double immunofluorescent immunohistochemistry. Fresh resection specimens were embedded in Tissue-Tek OCT compound (Sakura

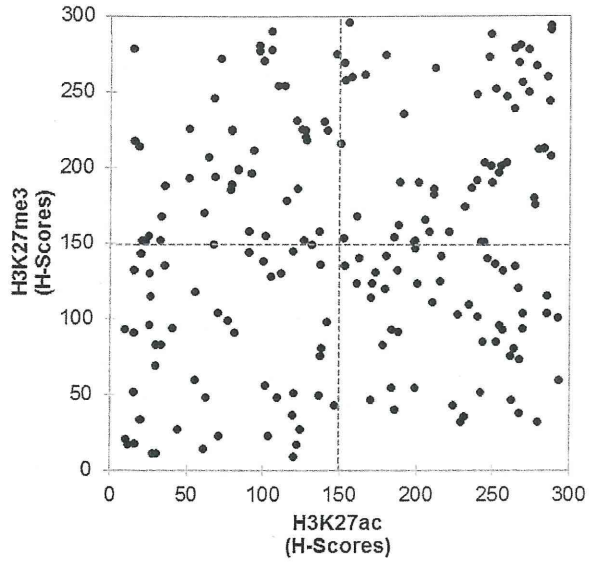

Figure 2. Distributions of histological scores (H-scores) of H3K27ac and H3K27me3 in HCC. H-score of 150 is shown in dashed lines.
doi:10.1371/journal.pone.0091330.g002

Finetek, Torrance, CA, USA) and frozen in a dry-ice acetone bath. Samples were kept at −80°C until analysis.

Immunohistochemistry

Whole tissue and TMA blocks were sectioned in 4 μm thickness and stained with a mouse monoclonal antibody against H3K27ac generated by one of the authors (CMA309; Hiroshi Kimura Laboratory; 1 μg/mL) and rabbit monoclonal antibody against H3K27me3 (#9733; Cell Signaling Technology, Beverly, MA, USA; 1:200 dilution). The reliability and specificity of the anti-H3K27ac antibody were examined in a previous study [21]. Immunohistochemical staining was performed according to standard techniques on a Ventana Benchmark XT autostainer (Ventana Medical Systems Inc., Tucson, AZ, USA). The appropriate positive and negative controls were included.

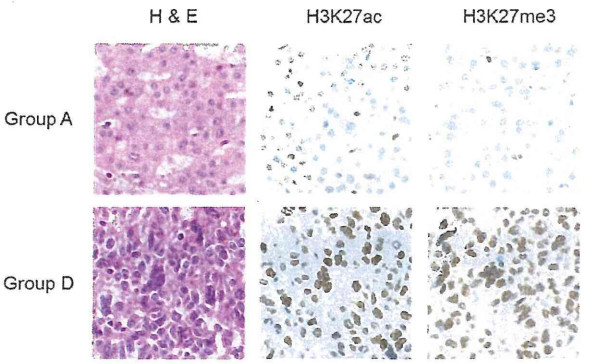

Figure 3. Images of H&E staining and H3K27ac and H3K27me3 immunohistochemistry of Group A (low-H3K27ac/low-H3K27me3) and Group D cases (high-H3K27ac/high-H3K27me3).
doi:10.1371/journal.pone.0091330.g003

Whole section slides of all cases were also immunostained with anti-p53 antibody (NCL-p53-505; Novocastra Laboratories, Newcastle, UK; 1:50 dilution) and anti-β-catenin antibody (610154; BD Transduction Laboratories, Lexington, KY, USA; 1:300 dilution) using the same protocols.

Western blotting

Frozen samples were sliced and lysed in lysis buffer (10 mmol/L Tris-HCl, pH 7.4, 150 mmol/L NaCl, 5 mmol/L EDTA, 1.0% Triton X-100, 1.0% sodium deoxycholate, 0.1% SDS, and 1 mmol/L of phenylmethylsulfonyl fluoride with protease inhibitor cocktail). Protein samples were loaded (10 μg of protein per lane) and fractionated on a 12% SDS polyacrylamide gel. After transfer onto a polyvinylidene difluoride membrane, membranes were probed with anti-H3K27ac (0.4 μg/mL) and anti-H3K27me3 (1:1000 dilution) antibodies. The membranes were visualized using the ECL Plus Western Blotting Detection System (GE Healthcare UK, Little Chalfont, UK). Hybridization with anti actin-β antibody (A5441; Sigma, Munich, Germany; 1:20000) was used as a loading control.

Evaluation of immunohistochemistry

After all slides were digitalized with a digital slide scanner (Nano Zoomer, Hamamatsu Photonics, Shizuoka, Japan), immunohistochemical results were scored with an image analyzing program (Tissue Studio, Definiens AG, Munich, Germany) [16]. Lymphocytes were used as internal positive controls in each case. Histological scores (H-scores) were determined as discussed in previous studies [22–24]. In brief, the H-score was calculated by multiplying the percentage of positive cells (0 to 100%) by the classified immunohistochemical marker intensity (0 to 3; as shown in **Figure 1a**). The H-scores ranged from 0 to 300. Most of the inflammatory cells and endothelial cells were excluded in this analysis by size and geometry selection of the analyzing program.

Intranuclear p53 or β-catenin positive staining was judged as positive/negative, according to standards described in the previous report [25].

Double immunofluorescent immunohistochemistry

To examine the localization of H3K27ac and H3K27me3 in nuclei, we performed double immunofluorescent immunohistochemistry in frozen samples. Whole tissue sections were incubated for 2 hours at room temperature with rabbit monoclonal anti-H3K27me3 antibody (1:200 dilution) along with mouse monoclonal anti-H3K27ac antibody (2 μg/mL). After washes, sections were incubated with Alexa Fluor 488 goat anti-mouse IgG (Invitrogen, Molecular Probes, Carlsbad, CA, USA; 1:1000) and Alexa Fluor 594 goat anti-rabbit IgG (Invitrogen; 1:1000) at room temperature for 1 hour. The immunolabeled frozen sections were observed with a Leica TCS SP5 spectral scanning confocal microscope (Leica Microsystems, Mannheim, Germany). Captured images of immunolabeled frozen sections were analyzed by Leica Application Suite (LAS) (Leica Microsystems, Mannheim, Germany), as previously described [26].

Statistical analysis

All statistical analyses except the time-dependent receiver operating characteristic (ROC) analysis were performed using JMP Pro 10 (SAS Institute Inc., Cary, NC, USA). Differences were considered significant at $P<0.05$. Categorical data were analyzed using two-sided Fisher's exact test. The Kaplan-Meier method and log-rank test were used to analyze survival. For multi-group comparison in the Kaplan-Meier method, the Bonferroni adjust-